



Temporal characteristics of atmospheric ammonia and nitrogen dioxide over China based on emission data, satellite observations and atmospheric transport modeling since 1980

Lei Liu¹, Xiuying Zhang¹, Wen Xu², Xuejun Liu², Yi Li³, Xuehe Lu¹, Yuehan Zhang⁴, and Wuting Zhang^{1,5}

¹Jiangsu Provincial Key Laboratory of Geographic Information Science and Technology, International Institute for Earth System Science, Nanjing University, Nanjing 210023, China

²College of Resources and Environmental Sciences, Centre for Resources, Environment and Food Security, Key Lab of Plant-Soil Interactions of MOE, China Agricultural University, Beijing 100193, China

³Air Quality Division, Arizona Department of Environmental Quality, Phoenix, AZ 85007, USA

⁴School of Atmospheric Sciences, Nanjing University, Nanjing, China

⁵Jiangsu Center for Collaborative Innovation in Geographical Information Resource Development and Application, Nanjing 210023, China

Correspondence to: Xiuying Zhang (lzhxy77@163.com)

Received: 3 February 2017 – Discussion started: 21 March 2017

Revised: 16 June 2017 – Accepted: 10 July 2017 – Published: 7 August 2017

Abstract. China is experiencing intense air pollution caused in large part by anthropogenic emissions of reactive nitrogen (N_r). Atmospheric ammonia (NH_3) and nitrogen dioxide (NO_2) are the most important precursors for N_r compounds (including N_2O_5 , HNO_3 , HONO and particulate NO_3^- and NH_4^+) in the atmosphere. Understanding the changes in NH_3 and NO_2 has important implications for the regulation of anthropogenic N_r emissions and is a requirement for assessing the consequence of environmental impacts. We conducted the temporal trend analysis of atmospheric NH_3 and NO_2 on a national scale since 1980 based on emission data (during 1980–2010), satellite observation (for NH_3 since 2008 and for NO_2 since 2005) and atmospheric chemistry transport modeling (during 2008–2015).

Based on the emission data, during 1980–2010, significant continuous increasing trends in both NH_3 and NO_x were observed in REAS (Regional Emission inventory in Asia, for NH_3 0.17 and for NO_x 0.16 kg N ha⁻¹ yr⁻²) and EDGAR (Emissions Database for Global Atmospheric Research, for NH_3 0.24 and for NO_x 0.17 kg N ha⁻¹ yr⁻²) over China. Based on the satellite data and atmospheric chemistry transport model (CTM) MOZART-4 (Model for Ozone and Related chemical Tracers, version 4), the NO_2 columns over China increased significantly from 2005 to 2011 and

then decreased significantly from 2011 to 2015; the satellite-retrieved NH_3 columns from 2008 to 2014 increased at a rate of 2.37 % yr⁻¹. The decrease in NO_2 columns since 2011 may result from more stringent strategies taken to control NO_x emissions during the 12th Five Year Plan, while no control policy has focused on NH_3 emissions. Our findings provided an overall insight into the temporal trends of both NO_2 and NH_3 since 1980 based on emission data, satellite observations and atmospheric transport modeling. These findings can provide a scientific background for policy makers that are attempting to control atmospheric pollution in China. Moreover, the multiple datasets used in this study have implications for estimating long-term N_r deposition datasets to assess its impact on soil, forest, water and greenhouse balance.

1 Introduction

Reactive nitrogen (N_r) emissions have increased significantly in China due to anthropogenic activities such as increased combustion of fossil fuels, over-fertilization and high stocking rates of farm animals (Canfield et al., 2010; Galloway et al., 2008; Liu et al., 2013). Elevated N_r in the environment has led to a series of effects on climate change and

ecosystems, e.g., biodiversity loss, stratospheric ozone depletion, air pollution, freshwater eutrophication, the potential alteration of global temperature, drinking water contamination, dead zones in coastal ecosystems and grassland seed bank depletion (Basto et al., 2015; Lan et al., 2015; Shi et al., 2015). Atmospheric reactive N emissions are dominated by nitrogen oxides ($\text{NO}_x = \text{NO} + \text{NO}_2$) and ammonia (NH_3 ; Li et al., 2016; Galloway et al., 2004). Atmospheric NO_2 and NH_3 are the most important precursors for N_r compounds including N_2O_5 , HNO_3 , HONO and particulate NO_3^- and NH_4^+ in the atmosphere (Xu et al., 2015; Pan et al., 2012). Therefore, an understanding of both the spatial and temporal patterns of NO_2 and NH_3 is essential for evaluating N-enriched environmental effects, and can provide the scientific background for N pollution mitigation.

To investigate the spatial and temporal variations in atmospheric NO_2 and NH_3 , ground measurements are acknowledged to be an effective way of monitoring the accurate concentrations of NO_2 and NH_3 (Xu et al., 2015; Pan et al., 2012; Meng et al., 2010). Ground measurements of NO_2 concentrations in China, including about 500 stations in 74 cities, have been monitored and reported to the public since January 2013 (Xie et al., 2015). By the end of 2013, this network was extended with hourly NO_2 concentrations from more than 850 stations in 161 cities. However, there are fewer NH_3 measurements across China than NO_2 measurements. The China Agricultural University has organized a nationwide nitrogen deposition monitoring network (NNDMN) since 2010, consisting of 43 monitoring sites covering urban, rural (cropland) and background (coastal, forest and grassland) areas across China (Xu et al., 2015; Liu et al., 2011). Xu et al. (2015) reported the ground NH_3 concentrations throughout China for the first time, providing great potential to understand the ground NH_3 concentrations on a national scale. Other networks include the Chinese Ecosystem Research Network (CERN) which was established in 1988, including 40 field stations (Fu et al., 2010). However, to our knowledge, there are no detailed reports about ground NH_3 concentrations from CERN on a national scale. In addition, four Chinese cities (Xiamen, Xi'an, Chongqing and Zhuhai) have joined the Acid Deposition Monitoring Network in East Asia (EANET) since 1999. However, only one site (Hongwen, Xiamen) in EANET measured the ground NH_3 concentrations, and the data from it are not continuous. Finally, ground NH_3 concentrations at 10 sites in northern China from 2007 to 2010 have been reported by Pan et al. (2012). All of the aboveground measurements provide the potential to understand NH_3 and NO_2 concentrations on a regional scale. However, there is limited information on the spatial and temporal variations in NH_3 and NO_2 in the atmosphere across China. This is due to the limited observation sites and monitoring period, as well as given the uneven distribution of the monitoring sites. Importantly, atmospheric NH_3 and NO_2 monitoring based on ground-based local sites may have limited spatial representativeness of the regional scale as both

NH_3 and NO_2 are highly variable in time and space (Clarisse et al., 2009; Wichink Kruit et al., 2012; Boersma et al., 2007).

In order to complement ground-based measurements, satellite observation of NH_3 and NO_2 is a welcome addition for analyzing the recent trends of NH_3 and NO_2 in the atmosphere. Satellite remote sensing offers an opportunity to monitor atmospheric NH_3 and NO_2 with high temporal and spatial resolutions (Warner et al., 2017; Li et al., 2017). NO_2 was measured by multiple space-based instruments, including the Global Ozone Monitoring Experiment (GOME), SCanning Imaging Absorption SpectroMeter for Atmospheric CHartographY (SCIAMACHY), Ozone Monitoring Instrument (OMI) and Global Ozone Monitoring Experiment-2 (GOME-2). The OMI NO_2 provides the best horizontal resolution ($13 \text{ km} \times 24 \text{ km}$) among instruments in its class and near-global daily coverage (Boersma et al., 2007). OMI observations have been widely applied in environmental-related studies and for the support of emission control policy (Russell et al., 2012; Zhao and Wang, 2009; Castellanos et al., 2015; Lamsal et al., 2015; F. Liu et al., 2016; Foy et al., 2016). First measurements of NH_3 from space were reported over Beijing and San Diego areas with the Tropospheric Emission Spectrometer (TES; Beer et al., 2008) and in fire plumes in Greece with the Infrared Atmospheric Sounding Interferometer (IASI; Coheur et al., 2009). The first global map of NH_3 was created from IASI measurements by correlating the observed brightness temperature differences to NH_3 columns using the averaged datasets in 2008 (Clarisse et al., 2009). Shortly after that, many studies focused on developing techniques to gain more reliable NH_3 columns (Whitburn et al., 2016a; Van Damme et al., 2014a), validating the retrieved NH_3 columns using the ground measurements (Van Damme et al., 2015; Dammers et al., 2016) and comparing the data with the results of the atmospheric chemistry transport models (Van Damme et al., 2014b; Whitburn et al., 2016a), and the estimated NH_3 columns obtained from Fourier transform infrared spectroscopy (FTIR; Dammers et al., 2016). The retrieval algorithm of obtaining IASI NH_3 columns was based on the method described in Whitburn et al. (2016a). Two main steps were performed to derive the NH_3 columns from the satellite measurements. First, derive the spectral hyperspectral range index (HRI) based on each IASI observations (Walker et al., 2011; Van Damme et al., 2014a). Second, convert HRI to NH_3 columns based on a constructed neural network with input parameters including vertical NH_3 profile, satellite viewing angle, surface temperature and so on (Whitburn et al., 2016a). The progress made in satellite techniques provides a possibility for understanding both the spatial and temporal variations in NH_3 and NO_2 in the atmosphere.

In addition to satellite observations, the emission data are also very important for investigating the temporal trends of NH_3 and NO_2 such as the IIASA inventory (Cofala et al., 2007), EDGAR (Emission Database for Global Atmospheric Research, RAINS-Asia (Regional Air Pollution Information

and Simulation) and Asia REAS (FRCGC, 2007). REAS is considered the first inventory to integrate historical, current and future emissions data for Asia based on a consistent methodology (Ohara et al., 2007), and EDGAR is the global emission data with 0.1 by 0.1 grid, which has the highest spatial resolution among different datasets mentioned above. Thus, REAS and EDGAR are used to analyze the historical trends of NH_3 and NO_2 during 1980–2010 in this study. Based on the EDGAR emission data, a widely used atmospheric transport model named as the Model for Ozone and Related chemical Tracers, version 4 (MOZART-4) was also used to model the temporal trend of NH_3 and NO_2 columns during 2008–2015 in comparison with the temporal trends of NH_3 and NO_2 columns measured by satellite instruments.

We aim at getting an overall insight into the temporal trends of both NO_2 and NH_3 since 1980 based on the multiple datasets including the emission data, satellite observations and atmospheric transport modeling. We herein show the Chinese national trend of REAS and EDGAR NH_3 and NO_x emission data during 1980–2010, satellite-retrieved NH_3 and NO_2 columns during 2008–2015 and 2005–2015, respectively, and atmospheric transport chemistry modeling of NH_3 and NO_2 columns during 2008–2015. It should be noted here that the satellite NH_3 columns were retrieved from the IASI, and can only be obtained since 2008. It is beneficial to analyze the temporal variations in both NH_3 and NO_2 , hence providing a scientific basis for policy makers to reduce N-enriched environmental pollution in China.

2 Materials and methods

2.1 NH_3 and NO_2 emissions

We examined the REAS (Regional Emission Inventory in Asia) emission inventory dataset for Asia with $0.5^\circ \times 0.5^\circ$ resolution for the period 1980–2010 and analyzed the temporal trends of NO_x and NH_3 over China. REAS v1.1 is believed to be the first inventory of integrating past, present and future dataset in Asia based on a consistent methodology. The REAS datasets have been validated by several emissions, and denote agreement with the recent growth status in Chinese emissions (Ohara et al., 2007). We also collected NO_x and NH_3 emission data from EDGAR (Emissions Database for Global Atmospheric Research) v4.3.1, which was developed by the Netherlands Environmental Assessment Agency and European Commission Joint Research Centre (Jg et al., 2002). The EDGAR emissions are calculated on the basis of a point emissions inventory conducted by the International Energy Agency. EDGAR also covers a long time period (1980–2010), with the highest spatial resolution globally ($0.1^\circ \times 0.1^\circ$; <http://edgar.jrc.ec.europa.eu/overview.php?v=431>).

2.2 Satellite observations

IASI is a passive remote-sensing instrument operating in nadir mode that measures the infrared radiation emitted by the Earth's surface and the atmosphere (Clarisse et al., 2009). It covers the entire globe twice a day, crossing the Equator at a mean solar local time of 09:30 and 21:30 and has an elliptical footprint of 12 by 12 km up to 20 by 39 km depending on the satellite-viewing angle. In this study we use daytime satellite observations as these are more sensitive to NH_3 and are associated with a large positive thermal contrast and a significant amount of NH_3 (Van Damme et al., 2014a; Whitburn et al., 2016a). The availability of measurements is mainly driven by the cloud coverage as only observations with cloud coverage lower than 25 % are processed to be a good compromise between the number of data kept for the analysis and the bias due to the effect of clouds. As the quantity of daily data is not always sufficient to obtain meaningful distributions (due to cloud cover or the availability of the temperature profiles from the EUMETSAT operational processing chain; Van Damme et al., 2014a), it is more appropriate to consider monthly or yearly averages for this trend analysis. We consider IASI observations with a relative error below 100 % or an absolute error below 5×10^{15} molec cm^{-2} for analysis over China. For the error, the filtering depends on the use of the data. For this, low columns typical for background conditions with a large relative error but a small absolute error are also taken into account. For other applications, such as comparing with ground measurements, we would recommend to use a threshold of 75 % or even 100 % relative error. We gained the data upon request from the Atmospheric Spectroscopy Group at Université Libre De Bruxelles (<http://www.ulb.ac.be/cpm/atmosphere.html>). These data can be gridded on 0.1° latitude \times 0.1° longitude (Dammers et al., 2016), 0.25° latitude \times 0.25° longitude (Whitburn et al., 2016a) and 0.5° latitude \times 0.5° longitude (Whitburn et al., 2016b) or even coarser resolutions depending on the usage of the data. For IASI NH_3 , we firstly divided China into a 0.5° latitude \times 0.5° longitude grid. For each grid cell, we calculated the monthly arithmetic mean by averaging the daily values with observations points within the grid cell. Similarly, we calculated the annual arithmetic mean by averaging the daily values with observations points within the grid cell over the whole year.

The NO_2 columns are obtained from the OMI instrument on NASA's EOS Aura satellite globally every day. We used the generated products by the project "Derivation of Ozone Monitoring Instrument tropospheric NO_2 in near-real time" (DOMINO) to analyze the temporal trends of NO_2 columns over China. In DOMINO products, only the observations with a cloud radiance fraction below 0.5 were processed for analysis. The retrieval algorithm is described in detail in the previous work (Boersma et al., 2007) and recent updates can be found in the DOMINO Product Specification Document (http://www.temis.nl/docs/OMI_NO2_HE5_

1.0.2.pdf). We used tropospheric NO_2 retrievals from the DOMINO algorithm v2.0. The retrieval quality of NO_2 products is strongly dependent on different aspects of air mass factors, such as radiative transfer calculations, terrain heights and surface albedo. The OMI v2.0 data were mainly improved by more realistic atmospheric profile parameters, and include more surface albedo and surface pressure reference points than before (Boersma et al., 2011, 2016). The DOMINO NO_2 datasets are available from <http://www.temis.nl/airpollution/no2.html>. We should state in particular that we used directly the DOMINO v2.0 products of monthly means from 2005 to 2015 over China for the trend analysis. The DOMINO NO_2 columns were gridded at a resolution of 0.125° latitude \times 0.125° longitude grid globally, which has been widely used for scientific applications (Ma et al., 2013; Ialongo et al., 2016; Castellanos et al., 2015).

To illustrate measurement availability, we presented here some measurement statistics. A total number of cloud-free daytime observations as characterized by the operational IASI processor by year were retrieved in China during 2008–2015 for NH_3 (Fig. 1b). We retrieved more observation numbers after 2010 than those during 2008–2009. In 2010, the update of the improved air temperature profiles, cloud properties products and cloud detection, which are important for calculating the thermal contrast, increased the quality of retrieval (Van Damme et al., 2014a, b). In September 2014, there was another update of the air temperature profiles, cloud properties products and cloud detection for calculating the thermal contrast. The version of IASI NH_3 columns used in the present work was based on the method described in Whitburn et al. (2016a). We did not use the IASI NH_3 after September 30 in 2014 for the trend analysis because an update of the input meteorological data on 30 September 2014 has caused a substantial increase in the retrieved atmospheric NH_3 columns. For the updates of the IASI- NH_3 data, the reader can refer to Van Damme et al. (2014a, b), and Whitburn et al. (2016a). The monthly observation numbers are also presented in Fig. 1a, showing that spring (March, April and May), summer (June, July and August), autumn (September, October and November) and winter (December, January and February) months represent 29, 26, 23 and 21 %, respectively. Compared with large variations in observation numbers for NH_3 , the observation numbers for NO_2 varied less by year; the winter season had the least, while other seasons varied little.

2.3 Atmospheric transport chemistry model

Atmospheric transport chemistry models are also of central importance in modeling the tropospheric NO_2 and NH_3 . We applied the widely used atmospheric global atmospheric transport chemistry model MOZART-4 to simulate the tropospheric NO_2 and NH_3 columns during 2008–2015 in accordance with the time period of IASI NH_3 measurements.

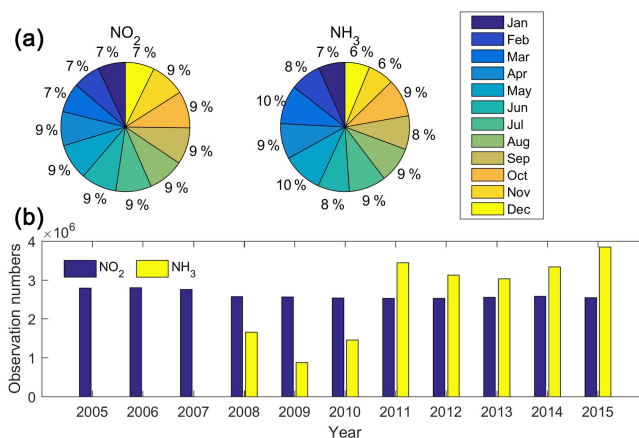


Figure 1. The satellite-derived observation numbers for NO_2 and NH_3 . Panel (a) shows the percentages of observations in each month in 2010 for NO_2 and in 2015 for NH_3 and (b) represents the total observation numbers for NO_2 and NH_3 over China. Notably, the NO_2 observation numbers were gained from DOMINO products with a cloud radiance fraction below 0.5, while the IASI observations with a relative error below 100 % or an absolute error below 5×10^{15} molec cm^{-2} were processed for analysis over China.

The MOZART-4 model is driven by the meteorological data from the NASA Goddard Earth Observing System Model, version 5 (GEOS-5), at a resolution of 1.9° latitude \times 2.5° longitude spatially. The emission data applied for driving the simulations are based on the updated EDGAR emission inventories. Twelve bulk aerosol compounds, 39 photolysis, 85 gas species and 157 gas-phase reactions were integrated in MOZART-4. The chemical mechanism on N compounds including the NO_2 , NH_3 and aerosols are detailedly integrated to MOZART-4, which is considered to be suitable for tropospheric chemical compositions (Emmons et al., 2010; Pfister et al., 2008; Sahu et al., 2013). The output data used in the current work temporally vary 6 h every day, which were available upon request from Louisa Emmons at the National Center for Atmospheric Research (NCAR). The monthly means of NO_2 and NH_3 columns were averaged by the daily data, and then used for the trend analysis over China. For more details about MOZART-4, the reader should refer to previous studies (Emmons et al., 2010; Brasseur et al., 1998; Beig and Singh, 2007).

3 Results and discussion

3.1 NH_3 and NO_2 emissions during 1980–2010

We conducted the temporal analysis of NH_3 and NO_x emissions since 1980 based on REAS and EDGAR. Significant continuous increasing trends in both NH_3 and NO_x were observed from REAS (for NH_3 0.17 and for NO_x 0.16 kg N ha^{-1} yr^{-2}) and EDGAR (for NH_3 0.24 and for

NO_x $0.17 \text{ kg N ha}^{-1} \text{ yr}^{-2}$) over China (Fig. 2). We found a relatively consistent increase in NO_x emission from EDGAR and REAS over China, i.e., $0.17 \text{ kg N ha}^{-1} \text{ yr}^{-2}$ vs. $0.16 \text{ kg N ha}^{-1} \text{ yr}^{-2}$, but inconsistency in the magnitude of NH_3 emissions from EDGAR and REAS over China, i.e., $0.24 \text{ kg N ha}^{-1} \text{ yr}^{-2}$ vs. $0.17 \text{ kg N ha}^{-1} \text{ yr}^{-2}$. The increase rate in NH_3 emissions over China from EDGAR was much higher than that from REAS, indicating that the magnitude of increase trend in NH_3 over China remains a debate, although their trend values (the slope in Fig. 2) of $0.24 \text{ kg N ha}^{-1} \text{ yr}^{-2}$ (EDGAR) vs. $0.17 \text{ kg N ha}^{-1} \text{ yr}^{-2}$ (REAS) both reflected a continuous increasing trend (in this regard they are consistent). It implies that the NH_3 emissions are indeed increasing during 1980–2010. We also conducted a simple correlation analysis of the NH_3 (Fig. 2a) and NO_x (Fig. 2b) from REAS and EDGAR, showing agreement in the magnitude (slope = 1.06) and temporal trend ($R^2 = 0.96$) for NO_x , but with some inconsistency in the increase rate (slope = 1.33) for NH_3 .

The discrepancy in the magnitude of NH_3 increase rate from REAS and EDGAR ($0.24 \text{ kg N ha}^{-1} \text{ yr}^{-2}$ vs. $0.17 \text{ kg N ha}^{-1} \text{ yr}^{-2}$) in China since 1980 may be caused by the different emission factors considered for estimating NH_3 emissions. The EDGAR v4.3.1 NH_3 emissions were calculated based on a variety of sectors, including agriculture, shipping, waste solid and wastewater, energy for buildings, process emissions during production and application, power industry, oil refineries, transformation industry, combustion for manufacturing, road transportation, railways, pipelines and off-road transport, while the REAS v1.1 NH_3 emissions focused mainly on agriculture sources (i.e., manure management of livestock and fertilizer application; Crippa et al., 2016; Ohara et al., 2007). Moreover, the fundamental methodology on estimating the REAS v1.1 NH_3 emissions did not consider the seasonal agricultural variations compared with that of EDGAR v4.3.1 NH_3 emissions (Kurokawa et al., 2013), and the removal efficiency (as a key element to estimate NH_3 emissions) was also reported to be much higher in REAS v1.1 than in EDGAR v4.3.1 (Kurokawa et al., 2013).

A previous study (Liu et al., 2013) summarized published data on the national anthropogenic NH_3 and NO_x emissions with multiple periods in China (Wang et al., 2009; Wang et al., 1997; Streets et al., 2003; Klimont et al., 2001; Sun and Wang, 1997; Olivier et al., 1998; FRCGC, 2007) and also analyzed the temporal pattern of NH_3 emissions. Their results showed that the NH_3 emissions had increased at an annual average rate of $0.32 \text{ Tg N yr}^{-2}$ (about $0.33 \text{ kg N ha}^{-1} \text{ yr}^{-2}$). The increase rate of NH_3 emissions ($0.33 \text{ kg N ha}^{-1} \text{ yr}^{-2}$) by Liu et al. (2013) was double that in REAS ($0.17 \text{ kg N ha}^{-1} \text{ yr}^{-2}$), implying that the NH_3 increase rate in China is still an open question and should be further studied.

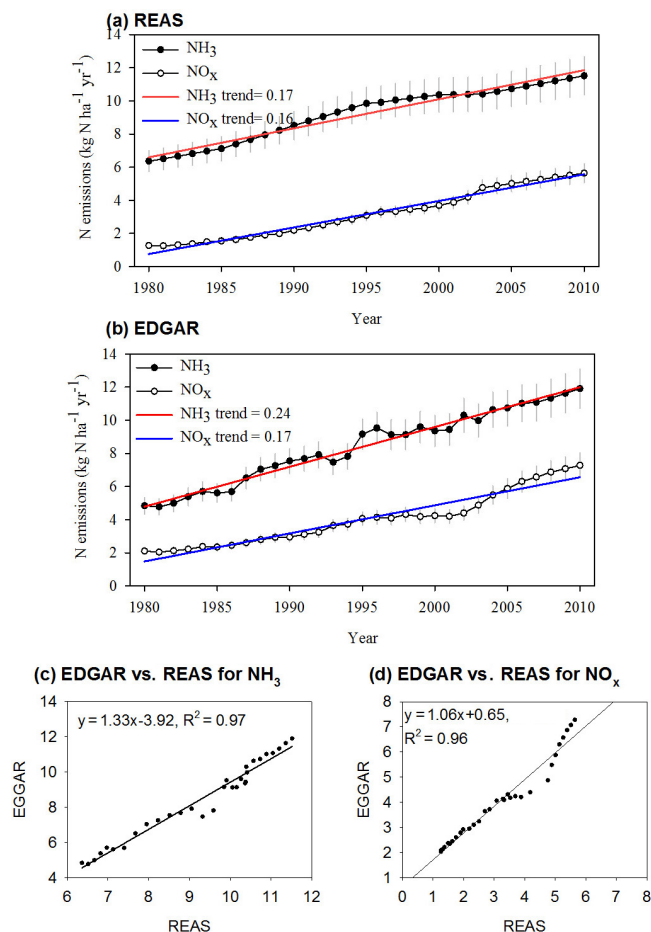


Figure 2. The NO_2 and NH_3 emissions over China. Panel (a) shows the NO_2 and NH_3 emissions over China from 1980 to 2010 from REAS, (b) represents the NO_2 and NH_3 emissions over China from 1980 to 2010 from EDGAR, (c) demonstrates the relationship of NO_2 emissions over China from REAS and EDGAR and (d) shows the relationship of NH_3 emissions over China from REAS and EDGAR.

3.2 Satellite NH_3 and NO_2 over China in the recent decade

3.2.1 Temporal trends

We referred to the method of a previous study (Russell et al., 2012) to conduct the temporal trend analysis by calculating the average values during cold months (October–March) and warm months (April–September), respectively. We herein concentrated more on the temporal analysis of satellite observations during warm months because of the relatively lower uncertainty in comparison with that during cold months. Figure 3 shows the temporal trend of NO_2 columns during warm and cold months between 2005 and 2015 as well as monthly average values. From satellite observations, the NO_2 columns over China increased with a slope of $0.063 \times 10^{15} \text{ molec cm}^{-2} \text{ yr}^{-1}$ ($4.07 \% \text{ yr}^{-1}$) in warm

months from 2005 to 2011 and then decreased with a slope of $-0.072 \text{ molec cm}^{-2}$ in warm months ($-3.62 \% \text{ yr}^{-1}$) from 2011 to 2015 (Fig. 3). The decreasing trends were consistent with NO_x emissions since 2011 over China (decreasing from $24.04 \times 10^6 \text{ t}$ in 2011 to $20.78 \times 10^6 \text{ t}$ in 2014, China Statistical Yearbook, <http://www.stats.gov.cn/>). During the 11th Chinese Five Year Plan (FYP) period (2006–2010), the Chinese government undertook a series of strategies to increase energy efficiency and to reduce NO_x emissions, but NO_x emissions were not successfully restrained, which created a big challenge for improving air quality over the country (Xia et al., 2016). During the 12th FYP period (2011–2015), more stringent strategies were implemented to control NO_x emissions, including the application of selective catalytic/non-catalytic reduction (SCR/SNCR) systems in the power sector; staged implementation of tighter vehicle emission standards; and a series of standards with aggressive emission limits for power, cement, and the iron and steel industries. These strategies are believed to have helped achieve national targets of NO_x emission abatement (Xia et al., 2016).

However, the satellite-retrieved NH_3 columns increased with a slope of $0.118 \times 10^{15} \text{ molec cm}^{-2} \text{ yr}^{-1}$ ($2.37 \% \text{ yr}^{-1}$) in warm months from 2008 to 2014 (Fig. 3). The percent increase rate for NH_3 by year ($2.37 \% \text{ yr}^{-1}$) from 2008 to 2014 is lower than that for NO_2 ($4.07 \% \text{ yr}^{-1}$) from 2005 to 2011, although the absolute NH_3 increase rate of $0.118 \times 10^{15} \text{ molec cm}^{-2} \text{ yr}^{-1}$ from 2008 to 2014 was higher than absolute NO_2 increase rate of $0.063 \times 10^{15} \text{ molec cm}^{-2} \text{ yr}^{-1}$ from 2005 to 2011. An increase in NH_3 columns from IASI may be due to decreased NH_3 removal, leading to a larger fraction maintained in the gaseous state for a long time rather than changing to the condensed phase. Specifically, NH_3 is considered an important alkaline gas that is abundant in the atmosphere and is able to neutralize acidic components such as HNO_3 and H_2SO_4 through the oxidation of NO_x and SO_2 , respectively (Li et al., 2014; Liu et al., 2011; X. Liu et al., 2017; Xu et al., 2015). The decreased NH_3 removal to some degree can be attributed to continuous decreased acidic gases, including NO_2 and SO_2 , over China under a strong control policy in 12th FYP, which can largely decrease the fraction of the chemical conversion to $(\text{NH}_4)_2\text{SO}_4$ and NH_4NO_3 in the atmosphere. A increasing trend in NH_3 columns may be associated with continuous N fertilizer use for guaranteeing an increase in crop production (Erisman et al., 2008). Although there was no strong NH_3 emission control regulation, N fertilizer efficiency should be further improved over China. In 2015, the Ministry of Agriculture formally announced its “Zero Increase Action Plan” for national fertilizer use by 2020, which requires that the annual increase in total fertilizer use be less than 1 % from 2015 to 2019, with no further increase from 2020 (Liu et al., 2015).

If the Zero Increase Action Plan for N fertilizer can be effective, future NH_3 emissions should be consistent with the current NH_3 emissions. In addition, due to strong emission

control of NO_x , the NO_x emissions were believed to decrease significantly from 2011 to 2015. We can reasonably make two major conclusions. First, the atmospheric NO_2 , as a key indicator of oxidized N compounds (NO_2 , HNO_3 and NO_3^-), decreased since 2011, and will continue to decrease under the current policy. Second, the atmospheric NH_3 , as a key indicator of reduced N (NH_3 and particulate NH_4^+), will slightly increase or stay at the current level in the future with the Zero Increase Action Plan. Thus, due to a decreasing trend of oxidized N ($\text{NO}_x\text{-N}$), ammonia N ($\text{NH}_x\text{-N}$) should still dominate N_r deposition (oxidized N plus reduced N) in China, and is expected to play a more significant role in N_r deposition. Therefore, monitoring the reduced N on a regional scale is encouraged to assist in enacting effective measures to protect the environments and public health, with respect to air, soil and water quality.

3.2.2 Spatial pattern

High NH_3 columns were found in Beijing, Hebei, Henan, Shandong, Hubei and Jiangsu provinces and in eastern Sichuan Province (Fig. 4a), which were consistent with their high NH_3 emissions due to intensive fertilizer application and livestock (Huang et al., 2012). Guangdong, Guangxi, Hunan and Jiangxi provinces also showed high NH_3 columns, due to high volatilization from paddy fields in these regions, with rice being the dominant crop and contributing the most emissions. High NH_3 columns in southern China are in agreement with the high percentage of paddy farmland area (Fig. S1a in the Supplement), and the high NH_3 columns in northern China are in agreement with the high percentage of dry farmland area (Fig. S1b). In addition, the NH_3 emissions from vehicles in urban areas could also contribute to the observed high NH_3 columns. For example, in Beijing, the contribution of vehicles equipped with catalytic converters, particularly since the introduction of three-way catalysts, to non-agricultural NH_3 emissions has recently been considered and might be the most important factor influencing NH_3 concentrations in urban cities (Meng et al., 2011; Xu et al., 2017). In addition, Xinjiang Province also emits remarkable NH_3 emissions related to sheep manure management (Huang et al., 2012; Kang et al., 2016; Zhou et al., 2015; Liu et al., 2017a). The lower NH_3 columns are located mostly in the Tibetan Plateau area, where there is a minimal amount of arable land and low use of synthetic nitrogenous fertilizers.

NO_2 columns (Fig. 4b) show significantly higher values over vast areas covering North China, East China, and the Sichuan Basin. The NO_2 columns also show high values over the Pearl River Delta, the southern part of Northeast China, and some areas in Northwest China. High NO_2 columns are mostly distributed in populated areas (Fig. S2), where there is a mix of various anthropogenic NO_x sources, such as vehicles and industrial complexes (Wang et al., 2012; Xu et al., 2015; Meng et al., 2010). It should be noted that an enhanced

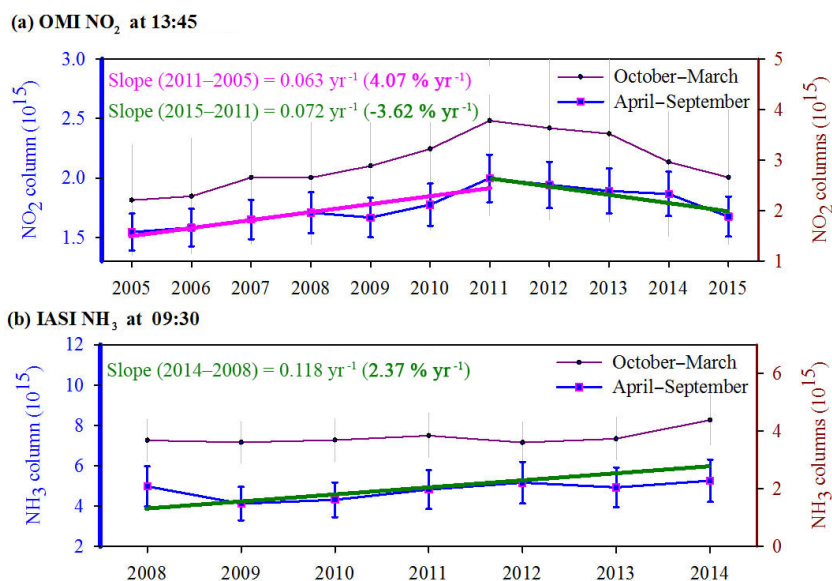


Figure 3. Time series of average OMI NO₂ and IASI NH₃ columns over China during warm months (April–September) and cold months (October–March). The time period of NO₂ columns was from 2005 to 2015, while the time span of NH₃ columns was from 2008 to 2014 over China. The associated mean error for each period is presented here as error bars. The percent increase or decrease rate (%) was the long-term mean, calculated as $100 \times \left(\frac{Y_2 - Y_1}{Y_1} + \frac{Y_3 - Y_2}{Y_2} + \dots + \frac{Y_{n+1} - Y_n}{Y_n} \right) \times \frac{1}{n}$.

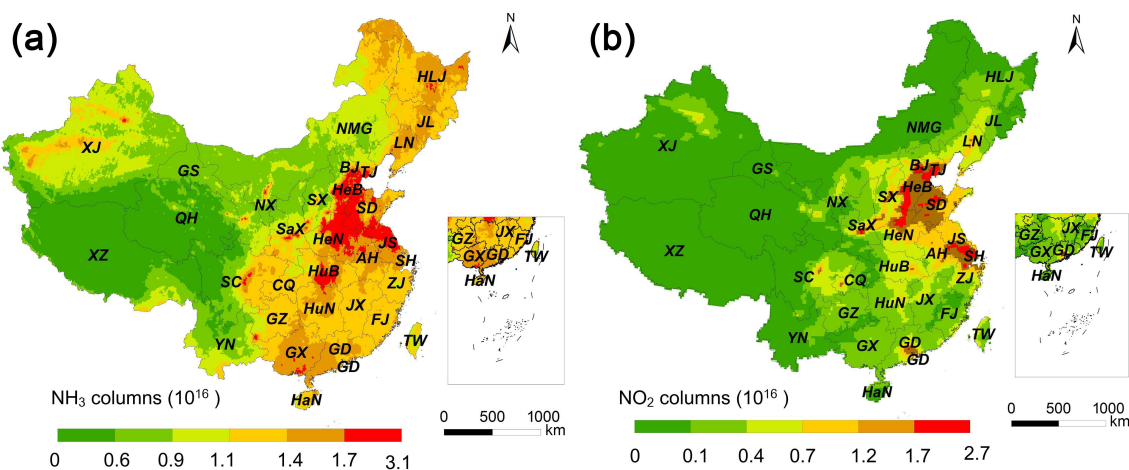


Figure 4. Spatial distribution of the annual NH₃ (a) and NO₂ (b) columns (molecules cm⁻² yr⁻¹). The full provincial names are Beijing (BJ), Tianjin (TJ), Hebei (HeB), Shandong (SD), Shanxi (SX), Henan (HeN), Shaanxi (SaX), Liaoning (LN), Jilin (JL), Heilongjiang (HLJ), Neimenggu (NMG), Gansu (GS), Ningxia (NX), Xinjiang (XJ), Shanghai (SH), Jiangsu (JS), Zhejiang (ZJ), Anhui (AH), Hubei (HuB), Hunan (HuN), Jiangxi (JX), Fujian (FJ), Guangdong (GD), Hainan (HaN), Yunnan (YN), Guizhou (GZ), Chongqing (CQ), Sichuan (SC), Guangxi (GX), Xizang (XZ) and Qinghai (QH).

emission intensity from transportation is confirmed since 2005, even with staged implementation of tightened emission standards for on-road vehicles (Wang et al., 2012). For example, NO_x emissions from transportation grew to 30 % for the whole country in 2014, and the values reached 44, 55, and 33 % for Beijing, Shanghai, and Guangdong, respectively (Xia et al., 2016). Therefore, transportation is believed to play an increasingly important role in regional NO₂ pollution, especially when emissions from stationary sources are

gradually controlled through increased penetration of selective catalytic/non-catalytic reduction (SCR/SNCR) systems.

3.2.3 Limitations of satellite observations

It is difficult to gain whole coverage over China based on the daily data for both IASI NH₃ and OMI NO₂. For daily NO₂, the spatial coverage gained by OMI was influenced by cloud radiance fractions, surface albedo, solar zenith angles,

row anomaly and so on (Russell et al., 2011; De Smedt et al., 2015). The “row anomaly” issue resulting from the OMI instrumental problem had an impact on approximately half of the rows undergoing unpredictable patterns in cross-track directions relying on latitudes and seasons and prevented obtaining convincing daily product with continuous coverage (Boersma et al., 2011, 2016). For NH_3 , the satellite instruments were strongly dependent on the meteorological conditions such as cloud fractions or the availability of the temperature profiles (Van Damme et al., 2014a; Boersma et al., 2011), and we cannot retrieve the whole coverage based on daily data over China. It will be beneficial to analyze a very local region with enough numbers of observations, but not appropriate to analyze such large coverage over China.

Facing this big challenge, we used the monthly data for the trend analysis over China. The uncertainty in DOMINO v2.0 NO_2 columns has been well documented in Boersma et al. (2011), and the relative error is reported lower than 20–30 % in East Asia by an improved altitude-dependent air mass factor look-up table, a more realistic atmospheric profile, an increased number of reference vertical layers and advanced surface albedos (Boersma et al., 2011). The reader is strongly suggested to refer to Boersma et al. (2011) for more details on the uncertainty analysis.

The potential uncertainty of IASI NH_3 columns resulted from IASI observation instruments and retrieval algorithms. In this paper, the NH_3 datasets were generated based on the recent-updated robust and flexible NH_3 retrieval algorithms, which were designed to overcome some shortcomings of the current algorithms (Whitburn et al., 2016a). The current algorithms were designed firstly to calculate the hyperspectral range index (HRI), a measure for the NH_3 signature strength in the spectrum, and then converted to IASI NH_3 columns by using the thermal contrast (TC) and look-up tables (LUTs) of the (HRI, TC) pair corresponding to NH_3 columns. The retrieval of HRIs is strongly dependent on the amount of NH_3 and the thermal state of the atmosphere (Whitburn et al., 2016a). The quality of the IASI NH_3 product has been validated by atmospheric chemistry transport models (CTMs), ground-based and airborne measurements, and NH_3 total columns obtained with ground-based Fourier transform infrared spectroscopy (FTIR). A first validation of the IASI NH_3 using the LOTOS-EUROS model was conducted over Europe, indicating the respective consistency of IASI measurements and model simulations (Van Damme et al., 2014b). A first evaluation of IASI NH_3 dataset using ground-based measurements was then made worldwide, presenting consistency with the available ground-based observations and denoting promising results for evaluation by using independent airborne data (Van Damme et al., 2015). A first validation of IASI NH_3 dataset using ground-based FTIR derived NH_3 total columns was evaluated, demonstrating a mean relative difference of $-32.4 \pm (56.3) \%$, a correlation r of 0.8 with a slope of 0.73 (Dammers et al., 2016).

3.3 Atmospheric chemistry transport model NO_2 and NH_3 columns since 2008

Satellite NO_2 and NH_3 columns were observed at overpass time as an instantaneous point in a day (at 09:30 for IASI NH_3 and at 13:45 for OMI NO_2 local time). These instantaneous satellite observations may not be representative of the temporal trend analysis over China. We further retrieved the monthly variations in NO_2 and NH_3 columns since 2008 from MOZART varying 6 h every day (00:00, 06:00, 12:00, 18:00). We compared the temporal trend analysis of NO_2 from MOZART at 12:00 with that gained from satellite at the overpass time (OMI 13:45 local time) as well as for NH_3 .

Figure 5 shows the NO_2 columns at 12:00 during warm and cold months between 2008 and 2015 from MOZART. The percent increase rate for NO_2 columns at 12:00 during warm months (April–September) between 2008 and 2011 was 4.02 \% yr^{-1} (Fig. 5), which was comparable with that (4.23 \% yr^{-1}) derived from OMI (Fig. 3). During 2011–2015, we found a slightly lower decrease rate (-2.93 \% yr^{-1}) in NO_2 columns during warm months at 12:00 from MOZART (Fig. 5) than that (-3.62 \% yr^{-1}) gained from OMI at 13:45 (Fig. 3). The temporal variations in NO_2 columns at 12:00 from MOZART were generally in accord with those from OMI at 13:45 local time. Figure 5 also demonstrates the average NO_2 columns (averaged at 00:00, 06:00, 12:00 and 18:00) during warm and cold months between 2008 and 2015. We found an increase rate at 12:00 (4.02 \%) close to that averaged at 00:00, 06:00, 12:00 and 18:00 (4.23 \%) before 2011, as well as a similar decrease rate at 12:00 (-2.93 \%) and average (-3.07 \%), implying that the temporal trend analysis at 12:00 vs. that averaged at 00:00, 06:00, 12:00 and 18:00 can be considered mostly consistent over China from MOZART.

For NH_3 , we found the percent increase rate at 12:00 during warm months between 2008 and 2015 was 1.30 \% yr^{-1} from MOZART (Fig. 5), which was lower than that (2.37 \% yr^{-1}) from IASI during 2008–2014. The percent increase rate by daily average (at 00:00, 06:00, 12:00 and 18:00) during warm months between 2008 and 2015 was 1.36 \% yr^{-1} from MOZART (Fig. 5). In MOZART-4, the alkaline gaseous NH_3 and the acidic gaseous NO_2 (the precursor for HNO_3) and SO_2 are very important precursors for bulk NH_4NO_3 and $(\text{NH}_4)_2\text{SO}_4$ particles, which form the primary system of gas–particle partitioning ($\text{NH}_3\text{--NH}_4^+\text{--NO}_x\text{--NO}_3^-\text{--SO}_2\text{--SO}_4^{2-}$). The chemical shifts between particulate NH_4NO_3 and gaseous NH_3 and NO_x are correlated with the abundance of NH_3 and NO_x and meteorological factors. The decreased abundance of NO_x between 2011 and 2015 may also contribute to an increase in the NH_3 abundance in the gas stage resulting from decreased conversion to particulate NH_4NO_3 .

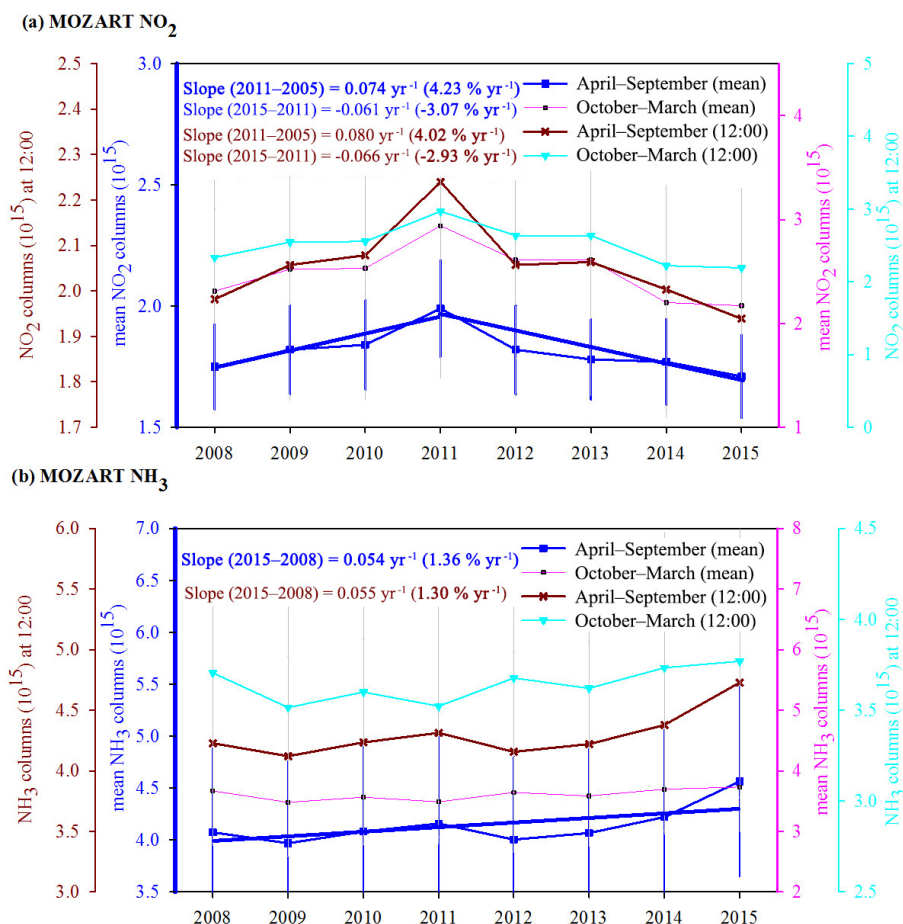


Figure 5. Time series of MOZART NO₂ and NH₃ columns over China during average warm months (April–September) and cold months (October–March) from 2008 to 2015. The mean columns were calculated by averaging the columns at 00:00, 06:00, 12:00 and 18:00. The associated mean error for each period is presented here as error bars.

3.4 Implications for estimating long-term N_r deposition datasets and recommendations for future work

We found both the NO_x and NH₃ over China increased continuously from 1980 to 2010 based on emissions data from REAS and EDGAR. In recent years, based on satellite observations, we found an increase of 2.37 % yr⁻¹ in NH₃ columns during 2008–2014. We also found high-level NO₂ columns over China from 2005–2011 (4.07 % yr⁻¹) but a decrease from 2011 to 2015 (-3.62 % yr⁻¹). Despite the decline, the NO₂ columns during 2011–2015 were still at a high level, with an average of 1.87×10^{15} molec cm⁻² yr⁻¹, compared with that (1.65×10^{15} molec cm⁻² yr⁻¹) during 2005–2010. Notably, these emissions certainly lead to the deposition of atmospheric N_r in the form of dry and wet processes into aquatic ecosystems and terrestrial, with implications of effects on ecosystem and human health, biological diversity and greenhouse gas balances (Lu et al., 2016). Hence, it is very crucial to estimate N_r deposition with high spatiotemporal resolutions in order to drive ecological models such

as the DeNitrification-DeComposition (DNDC) model and Integrated Biosphere Simulator (IBIS) to assess its impact on soil, forest, water and greenhouse balance. Here, we call for a long-term dataset of N_r depositions both regionally and globally to investigate how the N emissions affect the environment. A challenge still exists in estimating both the dry (NO₂, HNO₃ particulate NO₃⁻, NH₃ and particulate NH₄⁺) and wet (NH₄⁺ and NO₃⁻ in precipitation) depositions for a long-term dataset such as since 1980 or earlier, possibly due to the complex scheme of N transformations and transportation or limited available data from emissions, satellites and a limited number of ground measurements.

Satellite observations provide a new perspective for estimating N_r depositions regionally and have been used to improve the estimation performance. For example, to improve the modeling performance in dry gaseous NO₂ depositions from GEOS-Chem (Goddard Earth Observing System chemical transport model), Nowlan et al. (2014) applied the OMI NO₂ columns to calibrate the simulated ground NO₂ concentrations, and then estimated the deposition between 2005

and 2007. Our previous work focusing on the dry particulate NO_3^- deposition over China was also based on the OMI NO_2 columns, MOZART simulations and monitored-based sources (Liu et al., 2017b). Geddes et al. (2017) used the satellite NO_2 columns from GOME, GOME-2 and SCIAMACHY instruments to calibrate the NO_x emissions in GEOS-Chem to estimate the NO_x depositions since 1996. The simulations combining the satellite measurements and CTMs to derive N_r depositions (Geddes and Martin, 2017; Nowlan et al., 2014) in recent years will provide relatively accurate datasets (certainly need to be validated and modified by ground measurements).

Despite progress in satellite techniques in recent decades (for NO_2 since 1997 by GOME and for NH_3 since 2008 by IASI), we can find very few studies concerning N_r depositions before 1997 based on satellite observations. Thus, with the help of emissions data such as REAS and EDGAR, we can derive long-term N_r depositions, especially before 1997. Long-term emissions data such as REAS and EDGAR will provide a valuable dataset to expand the modeling of N_r depositions in recent years. In order to derive the N_r depositions from the emission data, CTMs are frequently used through modeling the wet (simplified as the product of scavenging efficiency and precipitation amount) and dry processes (simplified as the inferential method by multiplying the deposition velocity and gaseous or particulate concentrations). However, we still lack a comprehensive dataset of gridded long-term N_r depositions including both the dry (NO_2 , HNO_3 particulate NO_3^- , NH_3 and particulate NH_4^+) and wet (NH_4^+ and NO_3^- in precipitation) processes over China, which will be addressed in future work.

Another gap is that, all the abovementioned studies focused on the NO_x depositions and did not derive the NH_y (NH_3 and NH_4^+) depositions over China. Our recent work (Liu et al., 2017a) using IASI NH_3 columns combining the vertical profiles from MOZART benefits our understanding of the ground NH_3 concentrations over China, and the satellite-derived ground NH_3 concentrations were generally in accord with the national measurements from NNDMN. To date, there are still no reports of using the satellite NH_3 columns to derive the temporal and regional NH_y depositions over China, which dominated the total N_r depositions (NO_x plus NH_y ; L. Liu et al., 2016; Liu et al., 2013). The gaps in modeling of NH_y depositions by applying the satellite observations combining the CTM simulations require more efforts and further research.

4 Conclusions

Atmospheric ammonia (NH_3) and nitrogen dioxide (NO_2) play an important role in determining air quality, environmental degradation and climate change. The emission data, satellite observations and atmospheric transport modeling have great potential for understanding the temporal varia-

tions in atmospheric NH_3 and NO_2 on a regional scale, with high spatial and temporal resolutions. This study analyzed the characteristics of atmospheric NH_3 and NO_2 over China since 1980 based on the multiple datasets. The major findings were as follows:

1. Based on emission data, a significant continuous increasing trend in both NH_3 and NO_x were observed from REAS (for NH_3 0.17 and for NO_x 0.16 $\text{kg N ha}^{-1} \text{ yr}^{-2}$) and EDGAR (for NH_3 0.24 and for NO_x 0.17 $\text{kg N ha}^{-1} \text{ yr}^{-2}$) over China during 1980–2010.
2. Based on the satellite observations, we found high-level NH_3 columns with the percent increase rate of 2.37 % yr^{-1} from 2008 to 2014. For NO_2 , we found continuous high-level NO_2 columns over China from 2005–2011 but a decrease from 2011 to 2015 (still at a high level). The decrease of NO_2 columns may result from more stringent strategies taken to control NO_x emissions during the 12th Five Year Plan, including successful application of SCR/SNCR systems in the power sector, tighter emission standards on vehicles and a series of standards with aggressive emission limits. An increasing trend in NH_3 columns may be due to continuous N fertilizer use for guaranteeing a continuous increase in crop production. An increase in NH_3 columns may be due to decreased NH_3 removal leading to a larger fraction being maintained in the gaseous state for a long time rather than changing to the condensed phase, which may be related to continuously decreasing acidic gases, including NO_2 and SO_2 , over China under a strong control policy in 12th FYP.
3. Based on MOZART simulations, the temporal variations in NO_2 columns at 12:00 from MOZART were generally in accord with those from OMI at 13:45 local time. We also found a close increase rate at 12:00 (4.02 %) with that averaged at 00:00, 06:00, 12:00 and 18:00 (4.23 %) before 2011, as well as a similar decrease rate at 12:00 (−2.93 %) and the average (−3.07 %). For NH_3 , we found a lower percent increase rate from MOZART (1.30 % yr^{-1}) than IASI (2.37 % yr^{-1}) between 2008 and 2014.
4. The multiple datasets used in the current work have implications for estimating long-term N_r deposition datasets. The simulations combining the satellite measurements and CTMs to derive N_r depositions will provide relatively accurate datasets, and the REAS and EDGAR emissions have potential to expand the modeling N_r depositions to long-term datasets. In particular, modeling of NH_y depositions by applying satellite observations combining the CTM simulations requires more efforts and further research.

Data availability. All data sets related to this paper can be obtained by contacting the principal investigator, Xiuying Zhang (lzhy77@163.com).

The Supplement related to this article is available online at <https://doi.org/10.5194/acp-17-9365-2017-supplement>.

Competing interests. The authors declare that they have no conflict of interest.

Acknowledgements. We acknowledge the free use of tropospheric NO₂ column data from the OMI sensor from www.temis.nl. The NH₃ data were obtained by the Atmospheric Spectroscopy Group at Université Libre de Bruxelles (ULB; <http://www.ulb.ac.be/cpm/atmosphere.html>). Simon Whitburn and Martin Van Damme are acknowledged for making the data available and for their help in how to use them. We also thank Louisa Emmons from National Center for Atmospheric Research (NCAR) for providing the MOZART output data for the trend analysis. This study is supported by the National Natural Science Foundation of China (no. 41471343, 40425007 and 41101315).

Edited by: Jennifer G. Murphy

Reviewed by: two anonymous referees

References

- Basto, S., Thompson, K., Phoenix, G., Sloan, V., Leake, J., and Rees, M.: Long-term nitrogen deposition depletes grassland seed banks, *Nat. Commun.*, 6, 1–6, <https://doi.org/10.1038/ncomms7185>, 2015.
- Beer, R., Shephard, M. W., Kulawik, S. S., Clough, S. A., Eldering, A., Bowman, K. W., Sander, S. P., Fisher, B. M., Payne, V. H., Luo, M., Osterman, G. B., and Worden, J. R.: First satellite observations of lower tropospheric ammonia and methanol, *Geophys. Res. Lett.*, 35, L09801, <https://doi.org/10.1029/2008GL033642>, 2008.
- Beig, G. and Singh, V.: Trends in tropical tropospheric column ozone from satellite data and MOZART model, *Geophys. Res. Lett.*, 34, L17801, <https://doi.org/10.1029/2007GL030460>, 2007.
- Boersma, K. F., Eskes, H. J., Veeffkind, J. P., Brinkma, E. J., van der A, R. J., Sneep, M., van den Oord, G. H. J., Levelt, P. F., Stammes, P., Gleason, J. F., and Bucsela, E. J.: Near-real time retrieval of tropospheric NO₂ from OMI, *Atmos. Chem. Phys.*, 7, 2103–2118, <https://doi.org/10.5194/acp-7-2103-2007>, 2007.
- Boersma, K. F., Eskes, H. J., Dirksen, R. J., van der A, R. J., Veeffkind, J. P., Stammes, P., Huijnen, V., Kleipool, Q. L., Sneep, M., Claas, J., Leitão, J., Richter, A., Zhou, Y., and Brunner, D.: An improved tropospheric NO₂ column retrieval algorithm for the Ozone Monitoring Instrument, *Atmos. Meas. Tech.*, 4, 1905–1928, <https://doi.org/10.5194/amt-4-1905-2011>, 2011.
- Boersma, K. F., Vinken, G. C. M., and Eskes, H. J.: Representativeness errors in comparing chemistry transport and chemistry climate models with satellite UV-Vis tropospheric column retrievals, *Geosci. Model Dev.*, 9, 875–898, <https://doi.org/10.5194/gmd-9-875-2016>, 2016.
- Brasseur, G., Hauglustaine, D., Walters, S., Rasch, P., Müller, J. F., Granier, C., and Tie, X.: MOZART, a global chemical transport model for ozone and related chemical tracers: 1. Model description, *J. Geophys. Res.-Atmos.*, 103, 28265–28289, 1998.
- Canfield, D. E., Glazer, A. N., and Falkowski, P. G.: The Evolution and Future of Earth's Nitrogen Cycle, *Science*, 330, 192–196, <https://doi.org/10.1126/science.1186120>, 2010.
- Castellanos, P., Boersma, K. F., Torres, O., and de Haan, J. F.: OMI tropospheric NO₂ air mass factors over South America: effects of biomass burning aerosols, *Atmos. Meas. Tech.*, 8, 3831–3849, <https://doi.org/10.5194/amt-8-3831-2015>, 2015.
- Clarisse, L., Clerbaux, C., Dentener, F., Hurtmans, D., and Coheur, P.-F.: Global ammonia distribution derived from infrared satellite observations, *Nat. Geosci.*, 2, 479–483, 2009.
- Cofala, J., Amann, M., Klimont, Z., Kupiainen, K., and Höglund-Isaksson, L.: Scenarios of global anthropogenic emissions of air pollutants and methane until 2030, *Atmos. Environ.*, 41, 8486–8499, <https://doi.org/10.1016/j.atmosenv.2007.07.010>, 2007.
- Coheur, P.-F., Clarisse, L., Turquety, S., Hurtmans, D., and Clerbaux, C.: IASI measurements of reactive trace species in biomass burning plumes, *Atmos. Chem. Phys.*, 9, 5655–5667, <https://doi.org/10.5194/acp-9-5655-2009>, 2009.
- Crippa, M., Janssens-Maenhout, G., Dentener, F., Guizzardi, D., Sindelarova, K., Muntean, M., Van Dingenen, R., and Granier, C.: Forty years of improvements in European air quality: regional policy-industry interactions with global impacts, *Atmos. Chem. Phys.*, 16, 3825–3841, <https://doi.org/10.5194/acp-16-3825-2016>, 2016.
- Dammers, E., Palm, M., Van Damme, M., Vigouroux, C., Smale, D., Conway, S., Toon, G. C., Jones, N., Nussbaumer, E., Warneke, T., Petri, C., Clarisse, L., Clerbaux, C., Hermans, C., Lutsch, E., Strong, K., Hannigan, J. W., Nakajima, H., Morino, I., Herrera, B., Stremme, W., Grutter, M., Schaap, M., Wichink Kruit, R. J., Notholt, J., Coheur, P.-F., and Erisman, J. W.: An evaluation of IASI-NH₃ with ground-based Fourier transform infrared spectroscopy measurements, *Atmos. Chem. Phys.*, 16, 10351–10368, <https://doi.org/10.5194/acp-16-10351-2016>, 2016.
- De Smedt, I., Stavrou, T., Hendrick, F., Danckaert, T., Vlemmix, T., Pinardi, G., Theys, N., Lerot, C., Gielen, C., Vigouroux, C., Hermans, C., Fayt, C., Veeffkind, P., Müller, J.-F., and Van Roozendaal, M.: Diurnal, seasonal and long-term variations of global formaldehyde columns inferred from combined OMI and GOME-2 observations, *Atmos. Chem. Phys.*, 15, 12519–12545, <https://doi.org/10.5194/acp-15-12519-2015>, 2015.
- Emmons, L. K., Walters, S., Hess, P. G., Lamarque, J.-F., Pfister, G. G., Fillmore, D., Granier, C., Guenther, A., Kinnison, D., Laepple, T., Orlando, J., Tie, X., Tyndall, G., Wiedinmyer, C., Baughcum, S. L., and Kloster, S.: Description and evaluation of the Model for Ozone and Related chemical Tracers, version 4 (MOZART-4), *Geosci. Model Dev.*, 3, 43–67, <https://doi.org/10.5194/gmd-3-43-2010>, 2010.
- Erisman, J. W., Sutton, M. A., Galloway, J., Klimont, Z., and Winiwarter, W.: How a century of ammonia synthesis changed the world, *Nat. Geosci.*, 1, 636–639, 2008.

- Foy, B. D., Lu, Z., and Streets, D. G.: Satellite NO₂ retrievals suggest China has exceeded its NO_x reduction goals from the twelfth Five-Year Plan, *Scientific Reports*, 6, 35912, 2016.
- Fu, B., Li, S., Yu, X., Yang, P., Yu, G., Feng, R., and Zhuang, X.: Chinese ecosystem research network: Progress and perspectives, *Ecological Complexity*, 7, 225–233, <https://doi.org/10.1016/j.ecocom.2010.02.007>, 2010.
- Galloway, J. N., Dentener, F. J., Capone, D. G., Boyer, E. W., Howarth, R. W., Seitzinger, S. P., Asner, G. P., Cleveland, C. C., Green, P. A., Holland, E. A., Karl, D. M., Michaels, A. F., Porter, J. H., Townsend, A. R., and Vöös, C. J.: Nitrogen Cycles: Past, Present, and Future, *Biogeochemistry*, 70, 153–226, <https://doi.org/10.1007/s10533-004-0370-0>, 2004.
- Galloway, J. N., Townsend, A. R., Erisman, J. W., Bekunda, M., Cai, Z., Freney, J. R., Martinelli, L. A., Seitzinger, S. P., and Sutton, M. A.: Transformation of the Nitrogen Cycle: Recent Trends, Questions, and Potential Solutions, *Science*, 320, 889–892, <https://doi.org/10.1126/science.1136674>, 2008.
- Geddes, J. A. and Martin, R. V.: Global deposition of total reactive nitrogen oxides from 1996 to 2014 constrained with satellite observations of NO₂ columns, *Atmos. Chem. Phys. Discuss.*, <https://doi.org/10.5194/acp-2016-1100>, in review, 2017.
- Huang, X., Song, Y., Li, M., Li, J., Huo, Q., Cai, X., Zhu, T., Hu, M., and Zhang, H.: A high resolution ammonia emission inventory in China, *Global Biogeochem. Cy.*, 26, 1–14, 2012.
- Ialongo, I., Herman, J., Krotkov, N., Lamsal, L., Boersma, K. F., Hovila, J., and Tamminen, J.: Comparison of OMI NO₂ observations and their seasonal and weekly cycles with ground-based measurements in Helsinki, *Atmos. Meas. Tech.*, 9, 5203–5212, <https://doi.org/10.5194/amt-9-5203-2016>, 2016.
- Jg, O., Jm, B., Jahw, P., Bakker, J., Ajh, V., and Jpj, B.: Applications of EDGAR Emission Database for Global Atmospheric Research, *Rijksinstituut Voor Volksgezondheid En Milieu Rivm*, 2002.
- Kang, Y., Liu, M., Song, Y., Huang, X., Yao, H., Cai, X., Zhang, H., Kang, L., Liu, X., Yan, X., He, H., Zhang, Q., Shao, M., and Zhu, T.: High-resolution ammonia emissions inventories in China from 1980 to 2012, *Atmos. Chem. Phys.*, 16, 2043–2058, <https://doi.org/10.5194/acp-16-2043-2016>, 2016.
- Klimont, Z., Cofala, J., Schöpp, W., Amann, M., Streets, D. G., Ichikawa, Y., and Fujita, S.: Projections of SO₂, NO_x, NH₃ and VOC Emissions in East Asia Up to 2030, *Water Air Soil Poll.*, 130, 193–198, 2001.
- Kurokawa, J., Ohara, T., Morikawa, T., Hanayama, S., Janssens-Maenhout, G., Fukui, T., Kawashima, K., and Akimoto, H.: Emissions of air pollutants and greenhouse gases over Asian regions during 2000–2008: Regional Emission inventory in ASia (REAS) version 2, *Atmos. Chem. Phys.*, 13, 11019–11058, <https://doi.org/10.5194/acp-13-11019-2013>, 2013.
- Lamsal, L. N., Duncan, B. N., Yoshida, Y., Krotkov, N. A., Pickering, K. E., Streets, D. G., and Lu, Z.: U.S. NO₂ trends (2005–2013): EPA Air Quality System (AQS) data versus improved observations from the Ozone Monitoring Instrument (OMI), *Atmos. Environ.*, 110, 130–143, <https://doi.org/10.1016/j.atmosenv.2015.03.055>, 2015.
- Lan, Z., Jenerette, G. D., Zhan, S., Li, W., Zheng, S., and Bai, Y.: Testing the scaling effects and mechanisms of N-induced biodiversity loss: evidence from a decade-long grassland experiment, *J. Ecol.*, 103, 750–760, <https://doi.org/10.1111/1365-2745.12395>, 2015.
- Li, Y., Schwandner, F. M., Sewell, H. J., Zivkovich, A., Tigges, M., Raja, S., Holcomb, S., Molenar, J. V., Sherman, L., and Archuleta, C.: Observations of ammonia, nitric acid, and fine particles in a rural gas production region, *Atmos. Environ.*, 83, 80–89, 2014.
- Li, Y., Schichtel, B. A., Walker, J. T., Schwede, D. B., Chen, X., Lehmann, C. M., Puchalski, M. A., Gay, D. A., and Collett, J. L.: Increasing importance of deposition of reduced nitrogen in the United States, *P. Natl. Acad. Sci. USA*, 113, 5874–5879, 2016.
- Li, Y., Thompson, T. M., Van Damme, M., Chen, X., Benedict, K. B., Shao, Y., Day, D., Boris, A., Sullivan, A. P., Ham, J., Whitburn, S., Clarisse, L., Coheur, P.-F., and Collett Jr., J. L.: Temporal and spatial variability of ammonia in urban and agricultural regions of northern Colorado, United States, *Atmos. Chem. Phys.*, 17, 6197–6213, <https://doi.org/10.5194/acp-17-6197-2017>, 2017.
- Liu, F., Zhang, Q., Ronald, J. v. d. A., Zheng, B., Tong, D., Yan, L., Zheng, Y., and He, K.: Recent reduction in NO_x emissions over China: synthesis of satellite observations and emission inventories, *Environ. Res. Lett.*, 11, 114002, <https://doi.org/10.1088/1748-9326/11/11/114002>, 2016.
- Liu, L., Zhang, X., Wang, S., Lu, X., and Ouyang, X.: A Review of Spatial Variation of Inorganic Nitrogen (N) Wet Deposition in China, *PloS one*, 11, e0146051, <https://doi.org/10.1371/journal.pone.0146051>, 2016.
- Liu, L., Zhang, X., Xu, W., Liu, X., Lu, X., Wang, S., Zhang, W., and Zhao, L.: Ground Ammonia Concentrations over China Derived from Satellite and Atmospheric Transport Modeling, *Remote Sensing*, 9, 467, <https://doi.org/10.3390/rs9050467>, 2017a.
- Liu, L., Zhang, X., Zhang, Y., Xu, W., Liu, X., Zhang, X., Feng, J., Chen, X., Zhang, Y., Lu, X., Wang, S., Zhang, W., and Zhao, L.: Dry Particulate Nitrate Deposition in China, *Environ. Sci. Technol.*, 51, 5572, <https://doi.org/10.1021/acs.est.7b00898>, 2017b.
- Liu, X., Duan, L., Mo, J., Du, E., Shen, J., Lu, X., Zhang, Y., Zhou, X., He, C., and Zhang, F.: Nitrogen deposition and its ecological impact in China: An overview, *Environ. Pollut.*, 159, 2251–2264, <https://doi.org/10.1016/j.envpol.2010.08.002>, 2011.
- Liu, X., Zhang, Y., Han, W., Tang, A., Shen, J., Cui, Z., Vitousek, P., Erisman, J. W., Goulding, K., and Christie, P.: Enhanced nitrogen deposition over China, *Nature*, 494, 459–462, 2013.
- Liu, X., Vitousek, P., Chang, Y., Zhang, W., Matson, P., and Zhang, F.: Evidence for a Historic Change Occurring in China, *Environ. Sci. Technol.*, 50, 505–506, 2015.
- Liu, X., Xu, W., Duan, L., Du, E., Pan, Y., Lu, X., Zhang, L., Wu, Z., Wang, X., and Zhang, Y.: Erratum to: Atmospheric Nitrogen Emission, Deposition, and Air Quality Impacts in China: an Overview, *Current Pollution Reports*, 1–1, 2017.
- Lu, X., Jiang, H., Liu, J., Zhang, X., Jin, J., Zhu, Q., Zhang, Z., and Peng, C.: Simulated effects of nitrogen saturation on the global carbon budget using the IBIS model, *Scientific Reports*, 6, 39173, <https://doi.org/10.1038/srep39173>, 2016.
- Ma, J. Z., Beirle, S., Jin, J. L., Shaiganfar, R., Yan, P., and Wagner, T.: Tropospheric NO₂ vertical column densities over Beijing: results of the first three years of ground-based MAX-DOAS measurements (2008–2011) and satellite validation, *Atmos. Chem. Phys.*, 13, 1547–1567, <https://doi.org/10.5194/acp-13-1547-2013>, 2013.

- Meng, Z.-Y., Xu, X.-B., Wang, T., Zhang, X.-Y., Yu, X.-L., Wang, S.-F., Lin, W.-L., Chen, Y.-Z., Jiang, Y.-A., and An, X.-Q.: Ambient sulfur dioxide, nitrogen dioxide, and ammonia at ten background and rural sites in China during 2007–2008, *Atmos. Environ.*, 44, 2625–2631, <https://doi.org/10.1016/j.atmosenv.2010.04.008>, 2010.
- Meng, Z. Y., Lin, W. L., Jiang, X. M., Yan, P., Wang, Y., Zhang, Y. M., Jia, X. F., and Yu, X. L.: Characteristics of atmospheric ammonia over Beijing, China, *Atmos. Chem. Phys.*, 11, 6139–6151, <https://doi.org/10.5194/acp-11-6139-2011>, 2011.
- Nowlan, C., Martin, R., Philip, S., Lamsal, L., Krotkov, N., Marais, E., Wang, S., and Zhang, Q.: Global dry deposition of nitrogen dioxide and sulfur dioxide inferred from space-based measurements, *Global Biogeochem. Cy.*, 28, 1025–1043, 2014.
- Ohara, T., Akimoto, H., Kurokawa, J., Horii, N., Yamaji, K., Yan, X., and Hayasaka, T.: An Asian emission inventory of anthropogenic emission sources for the period 1980–2020, *Atmos. Chem. Phys.*, 7, 4419–4444, <https://doi.org/10.5194/acp-7-4419-2007>, 2007.
- Olivier, J. G. J., Bouwman, A. F., Hoek, K. W. V. D., and Berdowski, J. J. M.: Global air emission inventories for anthropogenic sources of NO_x , NH_3 and N_2O in 1990, *Environ. Pollut.*, 102, 135–148, 1998.
- Pan, Y. P., Wang, Y. S., Tang, G. Q., and Wu, D.: Wet and dry deposition of atmospheric nitrogen at ten sites in Northern China, *Atmos. Chem. Phys.*, 12, 6515–6535, <https://doi.org/10.5194/acp-12-6515-2012>, 2012.
- Pfister, G., Emmons, L., Hess, P., Lamarque, J. F., Orlando, J., Walters, S., Guenther, A., Palmer, P., and Lawrence, P.: Contribution of isoprene to chemical budgets: A model tracer study with the NCAR CTM MOZART-4, *J. Geophys. Res.-Atmos.*, 113, D05308, <https://doi.org/10.1029/2007JD008948>, 2008.
- FRCGC (Frontier Research Center for Global Change): Regional Emission Inventory in Asia, available at: <http://www.jamstec.go.jp/frsgc/research/d4/emission.htm> (last access: 1 August 2017), 2007
- Russell, A. R., Perring, A. E., Valin, L. C., Bucsele, E. J., Browne, E. C., Wooldridge, P. J., and Cohen, R. C.: A high spatial resolution retrieval of NO_2 column densities from OMI: method and evaluation, *Atmos. Chem. Phys.*, 11, 8543–8554, <https://doi.org/10.5194/acp-11-8543-2011>, 2011.
- Russell, A. R., Valin, L. C., and Cohen, R. C.: Trends in OMI NO_2 observations over the United States: effects of emission control technology and the economic recession, *Atmos. Chem. Phys.*, 12, 12197–12209, <https://doi.org/10.5194/acp-12-12197-2012>, 2012.
- Sahu, L., Sheel, V., Kajino, M., Gunthe, S. S., Thouret, V., Nedelec, P., and Smit, H. G.: Characteristics of tropospheric ozone variability over an urban site in Southeast Asia: A study based on MOZAIC and MOZART vertical profiles, *J. Geophys. Res.-Atmos.*, 118, 8729–8747, 2013.
- Shi, Y., Cui, S., Ju, X., Cai, Z., and Zhu, Y.-G.: Impacts of reactive nitrogen on climate change in China, *Scientific Reports*, 5, 8118, <https://doi.org/10.1038/srep08118>, 2015.
- Streets, D. G., Bond, T. C., Carmichael, G. R., Fernandes, S. D., He, D., Klimont, Z., Nelson, S. M., Tsai, N. Y., and Wang, M. Q.: An inventory of gaseous and primary aerosol emissions in Asia in the year 2000, *J. Geophys. Res.-Atmos.*, 108, 30–31, 2003.
- Sun, Q. and Wang, M.: Ammonia Emission and Concentration in the Atmosphere over China, *Scientia Atmospherica Sinica*, 1997.
- Van Damme, M., Clarisse, L., Heald, C. L., Hurtmans, D., Ngadi, Y., Clerbaux, C., Dolman, A. J., Erisman, J. W., and Coheur, P. F.: Global distributions, time series and error characterization of atmospheric ammonia (NH_3) from IASI satellite observations, *Atmos. Chem. Phys.*, 14, 2905–2922, <https://doi.org/10.5194/acp-14-2905-2014>, 2014a.
- Van Damme, M., Wichink Kruit, R., Schaap, M., Clarisse, L., Clerbaux, C., Coheur, P. F., Dammers, E., Dolman, A., and Erisman, J.: Evaluating 4 years of atmospheric ammonia (NH_3) over Europe using IASI satellite observations and LOTOS-EUROS model results, *J. Geophys. Res.-Atmos.*, 119, 9549–9566, 2014b.
- Van Damme, M., Clarisse, L., Dammers, E., Liu, X., Nowak, J. B., Clerbaux, C., Flechard, C. R., Galy-Lacaux, C., Xu, W., Neuman, J. A., Tang, Y. S., Sutton, M. A., Erisman, J. W., and Coheur, P. F.: Towards validation of ammonia (NH_3) measurements from the IASI satellite, *Atmos. Meas. Tech.*, 8, 1575–1591, <https://doi.org/10.5194/amt-8-1575-2015>, 2015.
- Walker, J. C., Dudhia, A., and Carboni, E.: An effective method for the detection of trace species demonstrated using the MetOp Infrared Atmospheric Sounding Interferometer, *Atmos. Meas. Tech.*, 4, 1567–1580, <https://doi.org/10.5194/amt-4-1567-2011>, 2011.
- Wang, S. W., Liao, J. H., Yu-Ting, H. U., and Yan, X. Y.: A Preliminary Inventory of NH_3 -N Emission and Its Temporal and Spatial Distribution of China, *Journal of Agro-Environment Science*, 2009.
- Wang, S. W., Zhang, Q., Streets, D. G., He, K. B., Martin, R. V., Lamsal, L. N., Chen, D., Lei, Y., and Lu, Z.: Growth in NO_x emissions from power plants in China: bottom-up estimates and satellite observations, *Atmos. Chem. Phys.*, 12, 4429–4447, <https://doi.org/10.5194/acp-12-4429-2012>, 2012.
- Wang, W. X., Lu, X. F., Pang, Y. B., Tang, D. G., and Zhang, W. H.: Geographical distribution of NH_3 emission intensities in China, *Actaentiae Circumstantiae*, 1997.
- Warner, J. X., Dickerson, R. R., Wei, Z., Strow, L. L., Wang, Y., and Liang, Q.: Increased atmospheric ammonia over the world's major agricultural areas detected from space, *Geophys. Res. Lett.*, 44, 2875–2884, <https://doi.org/10.1002/2016GL072305>, 2017.
- Whitburn, S., Van Damme, M., Clarisse, L., Bauduin, S., Heald, C. L., Hadji-Lazaro, J., Hurtmans, D., Zondlo, M. A., Clerbaux, C., and Coheur, P. F.: A flexible and robust neural network IASI- NH_3 retrieval algorithm, *J. Geophys. Res.-Atmos.*, 121, 6581–6599, <https://doi.org/10.1002/2016JD024828>, 2016a.
- Whitburn, S., Van Damme, M., Clarisse, L., Turquety, S., Clerbaux, C., and Coheur, P. F.: Doubling of annual ammonia emissions from the peat fires in Indonesia during the 2015 El Niño, *Geophys. Res. Lett.*, 43, 11007–11014, <https://doi.org/10.1002/2016GL070620>, 2016b.
- Wichink Kruit, R. J., Schaap, M., Sauter, F. J., van Zanten, M. C., and van Pul, W. A. J.: Modeling the distribution of ammonia across Europe including bi-directional surface–atmosphere exchange, *Biogeosciences*, 9, 5261–5277, <https://doi.org/10.5194/bg-9-5261-2012>, 2012.
- Xia, Y., Zhao, Y., and Nielsen, C. P.: Benefits of China's efforts in gaseous pollutant control indicated by the bottom-up emissions and satellite observations 2000–2014, *Atmos. Environ.*, 136, 43–53, <https://doi.org/10.1016/j.atmosenv.2016.04.013>, 2016.

- Xie, Y., Zhao, B., Zhang, L., and Luo, R.: Spatiotemporal variations of PM_{2.5} and PM₁₀ concentrations between 31 Chinese cities and their relationships with SO₂, NO₂, CO and O₃, *Particuology*, 20, 141–149, <https://doi.org/10.1016/j.partic.2015.01.003>, 2015.
- Xu, W., Luo, X. S., Pan, Y. P., Zhang, L., Tang, A. H., Shen, J. L., Zhang, Y., Li, K. H., Wu, Q. H., Yang, D. W., Zhang, Y. Y., Xue, J., Li, W. Q., Li, Q. Q., Tang, L., Lu, S. H., Liang, T., Tong, Y. A., Liu, P., Zhang, Q., Xiong, Z. Q., Shi, X. J., Wu, L. H., Shi, W. Q., Tian, K., Zhong, X. H., Shi, K., Tang, Q. Y., Zhang, L. J., Huang, J. L., He, C. E., Kuang, F. H., Zhu, B., Liu, H., Jin, X., Xin, Y. J., Shi, X. K., Du, E. Z., Dore, A. J., Tang, S., Collett Jr., J. L., Goulding, K., Sun, Y. X., Ren, J., Zhang, F. S., and Liu, X. J.: Quantifying atmospheric nitrogen deposition through a nationwide monitoring network across China, *Atmos. Chem. Phys.*, 15, 12345–12360, <https://doi.org/10.5194/acp-15-12345-2015>, 2015.
- Xu, W., Song, W., Zhang, Y., Liu, X., Zhang, L., Zhao, Y., Liu, D., Tang, A., Yang, D., Wang, D., Wen, Z., Pan, Y., Fowler, D., Collett Jr., J. L., Erisman, J. W., Goulding, K., Li, Y., and Zhang, F.: Air quality improvement in a megacity: implications from 2015 Beijing Parade Blue pollution control actions, *Atmos. Chem. Phys.*, 17, 31–46, <https://doi.org/10.5194/acp-17-31-2017>, 2017.
- Zhao, C. and Wang, Y.: Assimilated inversion of NO_x emissions over east Asia using OMI NO₂ column measurements, *Geophys. Res. Lett.*, 36, 1–5, 2009.
- Zhou, Y., Shuiyuan, C., Lang, J., Chen, D., Zhao, B., Liu, C., Xu, R., and Li, T.: A comprehensive ammonia emission inventory with high-resolution and its evaluation in the Beijing–Tianjin–Hebei (BTH) region, China, *Atmos. Environ.*, 106, 305–317, <https://doi.org/10.1016/j.atmosenv.2015.01.069>, 2015.